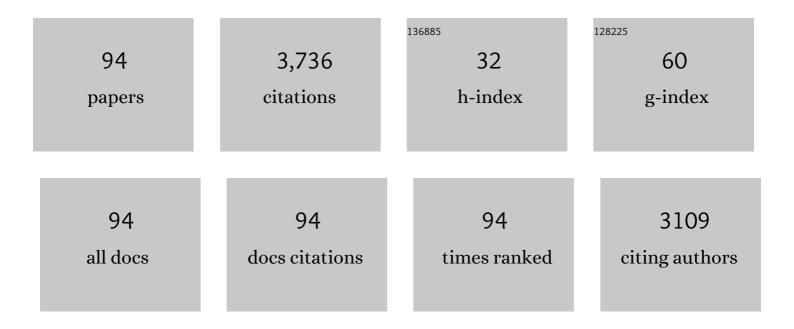
Scott C Davis

List of Publications by Year in descending order

Source: https://exaly.com/author-pdf/12144805/publications.pdf Version: 2024-02-01



#	Article	IF	CITATIONS
1	Near infrared optical tomography using NIRFAST: Algorithm for numerical model and image reconstruction. Communications in Numerical Methods in Engineering, 2009, 25, 711-732.	1.3	552
2	Pre-clinical whole-body fluorescence imaging: Review of instruments, methods and applications. Journal of Photochemistry and Photobiology B: Biology, 2010, 98, 77-94.	1.7	520
3	Image-guided diffuse optical fluorescence tomography implemented with Laplacian-type regularization. Optics Express, 2007, 15, 4066.	1.7	238
4	Spectrally resolved bioluminescence optical tomography. Optics Letters, 2006, 31, 365.	1.7	172
5	Magnetic resonance–coupled fluorescence tomography scanner for molecular imaging of tissue. Review of Scientific Instruments, 2008, 79, 064302.	0.6	161
6	Fast segmentation and high-quality three-dimensional volume mesh creation from medical images for diffuse optical tomography. Journal of Biomedical Optics, 2013, 18, 086007.	1.4	151
7	Revisiting photodynamic therapy dosimetry: reductionist & surrogate approaches to facilitate clinical success. Physics in Medicine and Biology, 2016, 61, R57-R89.	1.6	95
8	Cerenkov emission induced by external beam radiation stimulates molecular fluorescence. Medical Physics, 2011, 38, 4127-4132.	1.6	92
9	Projection imaging of photon beams by the ÄŒerenkov effect. Medical Physics, 2013, 40, 012101.	1.6	90
10	Dynamic dual-tracer MRI-guided fluorescence tomography to quantify receptor density in vivo. Proceedings of the National Academy of Sciences of the United States of America, 2013, 110, 9025-9030.	3.3	89
11	Three-dimensional ÄŒerenkov tomography of energy deposition from ionizing radiation beams. Optics Letters, 2013, 38, 634.	1.7	81
12	Subsurface diffuse optical tomography can localize absorber and fluorescent objects but recovered image sensitivity is nonlinear with depth. Applied Optics, 2007, 46, 1669.	2.1	79
13	Projection imaging of photon beams using ÄŒerenkov-excited fluorescence. Physics in Medicine and Biology, 2013, 58, 601-619.	1.6	79
14	Time-gated Cherenkov emission spectroscopy from linear accelerator irradiation of tissue phantoms. Optics Letters, 2012, 37, 1193.	1.7	74
15	Spectrally resolved bioluminescence tomography using the reciprocity approach. Medical Physics, 2008, 35, 4863-4871.	1.6	66
16	Techniques for fluorescence detection of protoporphyrin IX in skin cancers associated with photodynamic therapy. Photonics & Lasers in Medicine, 2013, 2, 287-303.	0.3	57
17	Maps of in vivo oxygen pressure with submillimetre resolution and nanomolar sensitivity enabled by Cherenkov-excited luminescence scanned imaging. Nature Biomedical Engineering, 2018, 2, 254-264.	11.6	55
18	Review of fluorescence guided surgery visualization and overlay techniques. Biomedical Optics Express, 2015, 6, 3765.	1.5	49

#	Article	IF	CITATIONS
19	Contrast-detail analysis characterizing diffuse optical fluorescence tomography image reconstruction. Journal of Biomedical Optics, 2005, 10, 050501.	1.4	47
20	MRI-coupled Fluorescence Tomography Quantifies EGFR Activity in Brain Tumors. Academic Radiology, 2010, 17, 271-276.	1.3	47
21	Dual-channel red/blue fluorescence dosimetry with broadband reflectance spectroscopic correction measures protoporphyrin IX production during photodynamic therapy of actinic keratosis. Journal of Biomedical Optics, 2014, 19, 075002.	1.4	45
22	Pulsed-light imaging for fluorescence guided surgery under normal room lighting. Optics Letters, 2013, 38, 3249.	1.7	44
23	ÄŒerenkov radiation emission and excited luminescence (CREL) sensitivity during external beam radiation therapy: Monte Carlo and tissue oxygenation phantom studies. Biomedical Optics Express, 2012, 3, 2381.	1.5	42
24	Comparing desferrioxamine and light fractionation enhancement of ALA-PpIX photodynamic therapy in skin cancer. British Journal of Cancer, 2016, 115, 805-813.	2.9	40
25	Video-rate optical dosimetry and dynamic visualization of IMRT and VMAT treatment plans in water using Cherenkov radiation. Medical Physics, 2014, 41, 062102.	1.6	39
26	ÄŒerenkov excited fluorescence tomography using external beam radiation. Optics Letters, 2013, 38, 1364.	1.7	38
27	5-Fluorouracil Enhances Protoporphyrin IX Accumulation and Lesion Clearance during Photodynamic Therapy of Actinic Keratoses: A Mechanism-Based Clinical Trial. Clinical Cancer Research, 2018, 24, 3026-3035.	3.2	38
28	Implicit and explicit prior information in near-infrared spectral imaging: accuracy, quantification and diagnostic value. Philosophical Transactions Series A, Mathematical, Physical, and Engineering Sciences, 2011, 369, 4531-4557.	1.6	36
29	Simultaneous <i>In Vivo</i> Fluorescent Markers for Perfusion, Protoporphyrin Metabolism, and EGFR Expression for Optically Guided Identification of Orthotopic Glioma. Clinical Cancer Research, 2017, 23, 2203-2212.	3.2	36
30	Fluorescence tomography characterization for sub-surface imaging with protoporphyrin IX. Optics Express, 2008, 16, 8581.	1.7	35
31	Multichannel diffuse optical Raman tomography for bone characterization in vivo: a phantom study. Biomedical Optics Express, 2012, 3, 2299.	1.5	35
32	Comparing implementations of magnetic-resonance-guided fluorescence molecular tomography for diagnostic classification of brain tumors. Journal of Biomedical Optics, 2010, 15, 051602.	1.4	34
33	Oxygen tomography by ÄŒerenkov-excited phosphorescence during external beam irradiation. Journal of Biomedical Optics, 2013, 18, 050503.	1.4	34
34	High Vascular Delivery of EGF, but Low Receptor Binding Rate Is Observed in AsPC-1 Tumors as Compared to Normal Pancreas. Molecular Imaging and Biology, 2012, 14, 472-479.	1.3	31
35	Topical dual-stain difference imaging for rapid intra-operative tumor identification in fresh specimens. Optics Letters, 2013, 38, 5184.	1.7	29
36	Dual-tracer background subtraction approach for fluorescent molecular tomography. Journal of Biomedical Optics, 2013, 18, 016003.	1.4	28

#	Article	IF	CITATIONS
37	Characterization and standardization of tissue-simulating protoporphyrin IX optical phantoms. Journal of Biomedical Optics, 2016, 21, 035003.	1.4	25
38	System development for high frequency ultrasound-guided fluorescence quantification of skin layers. Journal of Biomedical Optics, 2010, 15, 026028.	1.4	24
39	Detecting Epidermal Growth Factor Receptor Tumor Activity In Vivo During Cetuximab Therapy of Murine Gliomas. Academic Radiology, 2010, 17, 7-17.	1.3	22
40	Optimizing fresh specimen staining for rapid identification of tumor biomarkers during surgery. Theranostics, 2017, 7, 4722-4734.	4.6	21
41	White light-informed optical properties improve ultrasound-guided fluorescence tomography of photoactive protoporphyrin IX. Journal of Biomedical Optics, 2013, 18, 046008.	1.4	19
42	Tomography of epidermal growth factor receptor binding to fluorescent Affibody <i>in vivo</i> studied with magnetic resonance guided fluorescence recovery in varying orthotopic glioma sizes. Journal of Biomedical Optics, 2015, 20, 026001.	1.4	18
43	Heterogeneity of circulating tumor cell dissemination and lung metastases in a subcutaneous Lewis lung carcinoma model. Biomedical Optics Express, 2020, 11, 3633.	1.5	18
44	Optimization of fluorescent imaging in the operating room through pulsed acquisition and gating to ambient background cycling. Biomedical Optics Express, 2017, 8, 2635.	1.5	17
45	Observation of short wavelength infrared (SWIR) Cherenkov emission. Optics Letters, 2018, 43, 3854.	1.7	17
46	Noninvasive Optical Imaging of <scp>UV</scp> â€Induced Squamous Cell Carcinoma in Murine Skin: Studies of Early Tumor Development and Vitamin D Enhancement of Protoporphyrin <scp>IX</scp> Production. Photochemistry and Photobiology, 2015, 91, 1469-1478.	1.3	16
47	First experience imaging short-wave infrared fluorescence in a large animal: indocyanine green angiography of a pig brain. Journal of Biomedical Optics, 2019, 24, 1.	1.4	16
48	Hyperspectral imaging and spectral unmixing for improving whole-body fluorescence cryo-imaging. Biomedical Optics Express, 2021, 12, 395.	1.5	16
49	Diagnostic performance of receptor-specific surgical specimen staining correlates with receptor expression level. Journal of Biomedical Optics, 2019, 24, 1.	1.4	12
50	Assessing daylight & low-dose rate photodynamic therapy efficacy, using biomarkers of photophysical, biochemical and biological damage metrics in situ. Photodiagnosis and Photodynamic Therapy, 2017, 20, 227-233.	1.3	11
51	Cherenkov excited short-wavelength infrared fluorescence imaging in vivo with external beam radiation. Journal of Biomedical Optics, 2018, 24, 1.	1.4	11
52	Spectral distortion in diffuse molecular luminescence tomography in turbid media. Journal of Applied Physics, 2009, 105, 102024.	1.1	8
53	Tissue drug concentration determines whether fluorescence or absorption measurements are more sensitive in diffuse optical tomography of exogenous contrast agents. Applied Optics, 2009, 48, D262.	2.1	8
54	Noninvasive quantification of target availability during therapy using paired-agent fluorescence tomography. Theranostics, 2020, 10, 11230-11243.	4.6	8

#	Article	IF	CITATIONS
55	Characterizing short-wave infrared fluorescence of conventional near-infrared fluorophores. Journal of Biomedical Optics, 2019, 24, 1.	1.4	8
56	Prediction of optimal contrast times post-imaging agent administration to inform personalized fluorescence-guided surgery. Journal of Biomedical Optics, 2020, 25, .	1.4	8
57	Image-derived arterial input function for quantitative fluorescence imaging of receptor-drug binding <i>in vivo</i> . Journal of Biophotonics, 2016, 9, 282-295.	1.1	7
58	Probeâ€based fluorescence dosimetry of an antibodyâ€dye conjugate to identify head and neck cancer as a first step to fluorescenceâ€guided tissue preselection for pathological assessment. Head and Neck, 2020, 42, 59-66.	0.9	7
59	Correcting for targeted and control agent signal differences in paired-agent molecular imaging of cancer cell-surface receptors. Journal of Biomedical Optics, 2018, 23, 1.	1.4	5
60	A study of MRI-guided diffuse fluorescence molecular tomography for monitoring PDT effects in pancreas cancer. , 2009, , .		4
61	Time-gated Cherenkov emission spectroscopy from linear accelerator irradiation of tissue phantoms. , 2012, , .		4
62	Quantifying receptor density in vivo using a dual probe approach with fluorescence molecular imaging. , 2011, 7965, .		3
63	Small-Animal Imaging Using Diffuse Fluorescence Tomography. Methods in Molecular Biology, 2016, 1444, 123-137.	0.4	3
64	Clinically relevant dual probe difference specimen imaging (DDSI) protocol for freshly resected breast cancer specimen staining. BMC Cancer, 2021, 21, 440.	1.1	3
65	MRI-coupled spectrally resolved fluorescence tomography for in vivo imaging. , 2008, , .		2
66	Cherenkov-excited luminescence sheet imaging (CELSI) tomographic reconstruction. , 2017, , .		2
67	Effect of staining temperature on topical dual stain imaging of tissue specimens for tumor identification. , 2019, 10862, .		2
68	Noninvasive imaging of dual-agent uptake in glioma and normal tissue using MRI-coupled fluorescence tomography. , 2019, 10874, .		2
69	Modeling and image reconstruction in spectrally resolved bioluminescence tomography. , 2007, , .		1
70	EGF targeted fluorescence molecular tomography as a predictor of PDT outcomes in pancreas cancer models. , 2010, , .		1
71	MR-GUIDED PULSE OXIMETRY IMAGING OF BREAST IN VIVO. Journal of Innovative Optical Health Sciences, 2011, 04, 199-208.	0.5	1
72	Mathematical model to interpret localized reflectance spectra measured in the presence of a strong fluorescence marker. Journal of Biomedical Optics, 2016, 21, 061004.	1.4	1

#	Article	IF	CITATIONS
73	A hyperspectral approach for recovering agent excretion biodistributions using whole-body fluorescence cryo-imaging. , 2021, 11625, .		1
74	Image Reconstruction in Spectrally Resolved 3D Bioluminescence Tomography using the Adjoint Theorem. , 2008, , .		1
75	Quantifying cancer cell receptors with paired-agent fluorescent imaging: a novel method to account for tissue optical property effects. , 2018, 10497, .		1
76	On the use of fluorescein-based contrast agents as analogs to MRI-gadolinium agents for imaging brain tumors. , 2019, 10862, .		1
77	A paired-agent fluorescent molecular imaging strategy for quantifying antibody drug target engagement in in vivo window chamber xenograft models. , 2020, 11219, .		1
78	Developing a novel hyperspectral imaging cryomacrotome for whole body fluorescence imaging. , 2020, 11219, .		1
79	Estimating paired-agent uptake in altered tumor vasculature using MRI-coupled fluorescence tomography. , 2020, 11216, .		1
80	System design for spectrally encoded video-rate near infrared tomography during magnetic resonance imaging of the breast. Proceedings of SPIE, 2008, , .	0.8	0
81	Bioluminescence tomography using spectral techniques. , 2009, , .		Ο
82	MRI-guided fluorescence tomography of the breast: a phantom study. , 2009, , .		0
83	MRI-guided fluorescence tomography of PPIX in the breast: a case study. , 2011, , .		0
84	Double-excitation fluorescence spectral imaging: eliminating tissue auto-fluorescence from <i>in vivo</i> PPIX measurements. Proceedings of SPIE, 2012, , .	0.8	0
85	An ultrasound-guided fluorescence tomography system: design and specification. , 2013, , .		Ο
86	A method for validating depth-resolved biodistributions in topically-stained specimen with multi-channel fluorescence cryo-imaging. , 2021, 11625, .		0
87	Examining the Feasibility of Quantifying Receptor Availability Using Cross-Modality Paired-Agent Imaging. Molecular Imaging and Biology, 2021, , 1.	1.3	0
88	MRI-coupled fluorescence tomography of murine glioma metabolic activity. , 2008, , .		0
89	MRI-guided Fluorescence Molecular Tomography to Image Epidermal Growth Factor Receptor Status in Brain Tumors. , 2010, , .		0
90	Uptake of a fluorescence imaging agent in an orthotopic glioblastoma using fluorescence molecular tomography. , 2019, , .		0

#	Article	IF	CITATIONS
91	Diagnostic performance of receptor-specific surgical specimen staining correlate with receptor expression level. , 2019, 10862, .		0
92	Estimating drug delivery using hybrid system for simultaneous dynamic MRI and fluorescence tomography. , 2020, 11219, .		0
93	Monitoring cancer cell surface receptor expression during anti-angiogenesis therapy in vivo. Proceedings of SPIE, 2021, 11625, .	0.8	0
94	Whole-brain MR-registered cryo-imaging of a porcine-human glioma model to compare contrast agent biodistributions. , 2022, , .		0